RSC Advances

This is an *Accepted Manuscript*, which has been through the Royal Society of Chemistry peer review process and has been accepted for publication.

Accepted Manuscripts are published online shortly after acceptance, before technical editing, formatting and proof reading. Using this free service, authors can make their results available to the community, in citable form, before we publish the edited article. This *Accepted Manuscript* will be replaced by the edited, formatted and paginated article as soon as this is available.

You can find more information about *Accepted Manuscripts* in the Information for Authors.

Please note that technical editing may introduce minor changes to the text and/or graphics, which may alter content. The journal's standard Terms & Conditions and the Ethical guidelines still apply. In no event shall the Royal Society of Chemistry be held responsible for any errors or omissions in this *Accepted Manuscript* or any consequences arising from the use of any information it contains.

ROYAL SOCIETY OF CHEMISTRY

www.rsc.org/advances

Journal Name

RSCPublishing

ARTICLE

Multicomponent hybrids with surfactant-capped lanthanide polyoxometalate and ZIF-8 to tune luminescence

Cite this: DOI: 10.1039/x0xx00000x

Received 00th January 2012,
Accepted 00th January 2012

DOI: 10.1039/x0xx00000x

www.rsc.org/

Chang Liu, Bing Yan*

In this paper, two kinds of lanthanide polyoxometalates ($Na_9LnW_{10}O_{36}\cdot 32H_2O$, $K_{13}Ln(SiW_{11}O_{39})_2\cdot 30H_2O$ (Ln = Eu, Tb, Sm, Dy), abbreviated as LnW_{10} and $LnSiW_{11}$ respectively) are prepared and functionalized to surfactant-capped polyoxometalate ($SLnW_{10}$/$SLnSW_{11}$) using hexadecyltrimethyl ammonium bromide. Zeolitic imidazolate frameworks ZIF-8 nanoparticles are prepared and further composed with $SLnW_{10}$/$SLnSiW_{11}$. Both of inorganic components are fabricated into the process of polymerization reaction between ethyl methacrylate (EMA) and 4-vinyl pyridine (VPD) at the presence of initiator benzoyl peroxide to form multicomponent hybrids. The physical characterization and especially photoluminescence of these hybrid materials are studied in detail blow, whose luminescence color can be tuned and integrated by adjusting the building units. The result provides useful data to prepare multicomponent hybrid materials for practical optical application.

Introduction

Lanthanide inorganic/organic hybrid materials have attracted much more attentions in recent decades, because the combination of organic and inorganic components are both at the molecular and/or nanometer scale.[1] These materials possess together the advantages of organic compounds such as easy processing, flexibility, multifunctionality, as well hardness, thermal and chemical stability that derive from inorganic components. At present the studies are focused on the chemically bonded hybrids, which are constructed by strong and/or weak interactions such as covalent, ion-covalent, coordination, hydrogen bond and so forth.[2] Subsequently, a novel strategy so-called direct polymerization process is demonstrated to construct multicomponent hybrid materials.[3]

Polyoxometalates (POMs) are inorganic metal oxide clusters composed of transition metal ions that connected by oxygen with a few nanometer sizes. POMs not merely have well-defined molecular weight, nanostructure but also chemical, structural, and electronic versatility,[4] which can be used to construct large supramolecular systems as building blocks. These special properties make them play widely applications in catalysis, electrochemistry, semiconductors, and magnets *etc.* [5,6] As the examples of two kinds of lanthanide-doped POMs, 10-tungstoeuropate (9-) and bis-(11-tungstosilicato)europate (13-) anions as two different potassium salts have been firstly reported by Peacock and Weakley in 1971,[7] whose interesting luminescence properties catch attentions of the latter immediately to study extensively. Among the known luminescent POMs, $Na_9LnW_{10}O_{36}\cdot 32H_2O$ and $K_{13}Ln(SiW_{11}O_{39})_2\cdot 30H_2O$ possess the highest luminescent quantum yield.[8] The photoluminescent property of such POMs can help us to clearly understand the charge transfer transition state (LMCT) from oxygen to metal ion. In the above-POMs, inorganic $W_5O_{18}^{6-}$ and $W_{11}O_{39}^{8-}$ ions affect the coordination geometry of Ln^{3+} and result in the change of emission properties of Ln^{3+}.

However POMs are such kind of materials which can be dissolved in water generally and the processibility of pure POMs are inferior whether they are crystals or powders. In order to realize the assembly of POMs and other building blocks, it is necessary to modify POMs which depends on electrostatic interaction between extra cations and anions of POMs themselves.[9] In recent research, POMs can be phase transferred into organic media and functionalized by essential surfactants.[10] Therefore, as water-dissolved materials, POMs can be encapsulated into organic components of surfactants to obtain surfactant-capped POMs. The counter cations on the surface of POMs can be exchanged completely by cationic surfactants.[11] So the surfactant-capped POMs have the structure of a hydrophobic surfactant shell and an encapsulated hydrophilic POMs core by controlling a certain stoichiometric ratio in water/organic media. Then the surface properties of POMs are changed already and surfactant-capped POMs become soluble in organic media such as chloroform, benzene or toluene. Under this effective approach, it is readily to obtain some hybrid materials based with POMs.[12] POMs can be introduced into

RSC Advances Accepted Manuscript

polymer matrices, which can be expected to have promising behaviour such as easily processing and good stability.

Metal organic frameworks (MOFs) are a class of porous coordination polymers materials with a well-defined porous structure.[13] Porous zeolitic imidazolate frameworks (ZIFs), as a branch of metal organic frameworks which have exceptional chemical and thermal stability, have attracted impressive attention in the past few years for energy, storage and chemical applications.[13-15] In particular, ZIF-8 has the sodalite zeolite-type structure, small apertures (3.4 Å) and large cavities (11.6 Å),[14] whose nanoparticles exhibit unique properties that are distinct from both molecules and bulk solids. ZIF-8 possess the visible emission bands covering blue-green region, as a luminescent units can be introduced into the hybrid system and expected to integrate with POMs to realize the tuneable luminescence and even white luminescence. ZIF-8 nanoparticles are popular to choose for its cheap, nontoxic and chemically stable virtues. Moreover, ZIF-8 can be easily modified with polymer and connected with surfactant-capped POMs and polymer through polymerization[16].

In this paper, we firstly assemble the hybrid system including lanthanide POMs and zeolitic imidazolate frameworks (ZIF-8) and polymer. The detailed characterizations of the obtained materials are performed, and especially photophysical properties are discussed deeply.

Experimental Section

Materials

Four lanthanide nitrates $Ln(NO_3)_3 \cdot xH_2O$ (Ln = Eu, Tb, Sm, Dy) were synthesized by dissolving their oxides (Eu_2O_3, Tb_4O_7, Sm_2O_3, Dy_2O_3) into the concentrated nitric acid along with heating and stirring to accelerate the rate of reactions till the crystal film appeared. $Na_2WO_4 \cdot 2H_2O$ and $H_4[Si(W_3O_{10})_4] \cdot xH_2O$ were purchased from Aldrich. Hexadecyltrimethyl ammonium bromide (HTAB) and AcOK were from Shanghai Adamas Reagent Co., Ltd. The solvent tetrahydrofuran (THF) was used after desiccation with anhydrous magnesium sulfate. All the other reagents were analytically pure and used as received.

Synthetic procedures

Preparation of $Na_9LnW_{10}O_{36} \cdot 32H_2O$ (abbreviated as LnW_{10})

The synthesis method of LnW_{10} (Ln = Eu, Tb, Sm, Dy) was accorded to the report by Peacock and Weakly [7]. Here we used $Na_9EuW_{10}O_{36} \cdot 32H_2O$ (EuW_{10}) as example: a certain amount of $Na_2WO_4 \cdot 2H_2O$ (3.3 g, 10 mmol) was dissolved into 8 mL deionized water and the solution was heated to 85 °C, whose pH value is adjusted to about 7-8 using the glacial acetic acids. Then 1 mmol europium nitrate was also dissolved in 0.8 mL deionized water, and the solution of $Eu(NO_3)_3 \cdot xH_2O$ was added slowly into the above Na_2WO_4 solution. White precipitate appeared immediately and the solution was cooled to room temperature. The final powder products were filtered and dried in vacuum drying oven, named as EuW_{10}. The other three lanthanide tungstates $Na_9TbW_{10}O_{36} \cdot 32H_2O$ (TbW_{10}), $Na_9SmW_{10}O_{36} \cdot 32H_2O$ (SmW_{10}), $Na_9DyW_{10}O_{36} \cdot 32H_2O$ (DyW_{10}) were also prepared by replacing $Eu(NO_3)_3 \cdot xH_2O$ with $Tb(NO_3)_3 \cdot xH_2O$, $Sm(NO_3)_3 \cdot xH_2O$ and $Dy(NO_3)_3 \cdot xH_2O$, respectively.

Preparation of $K_{13}Ln(SiW_{11}O_{39})_2 \cdot 30H_2O$ (abbreviated as $LnSiW_{11}$)

The lanthanide-doped tungsten silicates $LnSiW_{11}$ (Ln = Eu, Sm, Dy) were also obtained on the basis of the method by Peacock and Weakly.[7] A typical experiment was described as follows: $H_4SiW_{12}O_{40}$ (5.7 g, 2 mmol) was dissolving into 20 mL deionized water and heated to 90 °C successively. Then the warm concentrated mixed solutions of $Eu(NO_3)_3 \cdot 6H_2O$ (0.4 g, 1 mmol) and AcOK (8.0 g, 80 mmol as the sources of potassium, pH ~ 7) were added dropwise in the above $H_4SiW_{12}O_{40}$ solutions. The light yellow solution was kept to stir about 5 minutes at 90 °C until the suspension of $K_7SiW_{11}O_{39}$ solved completely. A kind of colorless oil which separated and crystallized from the solution when set the temperature at 5 °C. The compound was recrystallized thrice from hot water. The final powder products were filtered and dried in vacuum drying oven and named as $EuSiW_{11}$. Other two lanthanide-doped tungsten silicate $K_{13}Sm(SiW_{11}O_{39})_2 \cdot 30H_2O$ ($SmSiW_{11}$), $K_{13}Dy(SiW_{11}O_{39})_2 \cdot 30H_2O$ ($DySiW_{11}$) were also prepared by replacing $Eu(NO_3)_3 \cdot xH_2O$ with their nitrates, respectively.

Preparation of zeoliticimidazolate frameworks (ZIF-8)

Solid state zinc nitrate hexahydrate $Zn(NO_3)_2 \cdot 6H_2O$ (1.5 g 5 mmol) and 2-methylimidazole (H-MeIM) (0.4 g 5 mmol) were successive dissolved in 75 mL of DMF. The solution was transferred in a 100 mL vial and heated to 140 °C in a programmable oven and kept at this temperature then cooled to room temperature after 24 h. The mother liquor was removed from the solution, and 20 mL of chloroform was added to the vial. Colorless polyhedral crystals were separated from the upper layer, washed with DMF three times, and dried in air to remove the excess DMF for 10 minutes.

The synthesis of surfactant-capped POMs (LnW_{10}/$LnSiW_{11}$) clusters (denoted as $SLnW_{10}$/$SLnSiW_{11}$)

Two kinds of polyoxometalate (POM) newly prepared were dissolved in aqueous solution and a proportion of chloroform solution of surfactant HTAB was added slowly with stirring according to the literature.[17] The initial molar ratio of HTAB to LnW_{10} was set as 9: 1 and HTAB to $LnSiW_{11}$ was 13: 1, respectively. The two polyoxometalates were extracted and transferred into chloroform solution after ions exchanged. The organic phase was separated by funnel, and $SLnW_{10}$/$SLnSiW_{11}$ was obtained by evaporating the organic phase to dry using rotary evaporator. The products were washed with deionized water for three times in order to remove the salts NaBr/KBr. After re-crystallization with ethanol, the final products were obtained as white powders.

The preparation of multi-component hybrids $SLnW_{10}$/$SLnSiW_{11}$, ZIF-8 and polymers PEMA (abbreviated as $SLnW_{10}$-ZIF-8-PEMA/$SLnSiW_{11}$-ZIF-8-PEMA)[18]

The sample of ZIF-8 was degassed and dried successively for 10 hrs at 426 K to remove the solvent molecules in their channels under vacuum. And then 200 mg ZIF-8 was added into 25 mL THF solution of the above-mentioned lanthanide complexes $SLnW_{10}$/$SLnSiW_{11}$ (the molar ratio of ZIF-8/$SLnW_{10}$ or ZIF-8/$SLnSiW_{11}$ was 9: 1). The reaction was agitated magnetically to disperse uniformly for 5 hrs at 313 K. And a certain volume of 4-vinylpyridine (VPD) was dropwise added to the above suspension and continued to react with each other for another 5 hrs (the final

RSC Advances Accepted Manuscript

This journal is © The Royal Society of Chemistry 2012

molar ratio of ZIF-8/SLnW$_{10}$/VPD or ZIF-8/SLnSiW$_{11}$/VPD was 9: 1: 2). Afterwards, 1 mL of liquid monomer EMA was then input to the above mixture, following with the aggregation initiator benzoyl peroxide (BPO). The amount of initiator was 0.4 – 0.5 % of the monomer. The mixed solution was kept agitated magnetically for approximately 6 hrs at 353 K under argon atmosphere to obtain the hybrids which were constructed through addition polymerization between VPD and EMA. The obtained materials were concentrated under the boiling point of THF to remove the excess solvent using a rotary vacuum evaporator, and the resulting products were viscous liquid. The elemental analyses data were shown in supporting information.

Preparations of SLnW$_{10}$-ZIF-8-PEMA/SLnSiW$_{11}$-ZIF-8-PEMA thin films

The luminescent polymer thin films of SLnW$_{10}$-ZIF-8-PEMA/SLnSiW$_{11}$-ZIF-8-PEMA were gained by direct spin-coating method. 1 mL of the above colloid was dissolved in proper amount of THF and dropped onto a cleaned 1 cm × 1 cm ITO glass which was fixed on a Laurell spin-coater. The spin rate and spin time were kept at 1000 rpm/min. The solvent was removed by drying the thin films at room temperature after spin-coating.

Physical measurements [19]

The powder X-ray diffraction (PXRD) patterns were acquired on a Bruker D8 diffractometer using Cu Kα radiation with 40 mA and 40 kV, the data were collected within the 2θ range of 5 – 65 °. Fourier transform infrared (FTIR) spectra were measured within the 4000-400 cm^{-1} region on a Nexus 912 AO446 spectrophotometer with the KBr pellet technique. The elemental analyses (C, H, N) of the ternary lanthanide hybrids were measured with a CARIO-ERBA 1106 elemental analyzer and the contents of metal element (Ln, Zn) were determined on the Perkin Optima 2100DV Inductively Coupled Plasma Optical Emission Spectrometer (ICP-OES). Photoluminescence spectra and luminescence lifetimes were detected by an Edinburgh FLS920 phosphorescent instrument. The outer absolute luminescent quantum efficiency was determined using an integrating sphere (150 mm diameter, $BaSO_4$ coating) from Edinburgh FLS920 phosphorimeter. The fluorescence spectra were corrected for variations in the output of the excitation source (a 450 W xenon lamp) and for variations in the detector response. The quantum yield can be defined as the integrated intensity of the luminescence signal divided by the integrated intensity of the absorption signal. The absorption intensity was calculated by subtracting the integrated intensity of the light source with the sample in the integrating sphere from the integrated intensity of the light source with a blank sample in the integrating sphere.

Results and Discussion

The PXRD patterns indicate that all the POMs with different lanthanide ions have the same crystal structure (Figure S1). Hexadecyltrimethyl ammonium bromide (HTAB) is a kind of cationic surfactant, which has an excellent ability of coordination with cationic, non-ionic and amphoteric surfactants. We outline the modification for the specific case of $Na_9LnW_{10}O_{36}\cdot 32H_2O$ (LnW$_{10}$) as this procedure is followed for the POMs. As shown in Figure 1a, surfactant-capped LnW$_{10}$ (SLnW$_{10}$) is prepared with the ion exchange between the surfactant HTAB and the LnW$_{10}$ for the electrostatic attraction force between their different charges.[20] A certain amount of LnW$_{10}$ is dissolved in water and surfactant HTAB chloroform solution (the molar ratio of HTAB to LnW$_{10}$ is 9: 1) is added slowly with stirring. After ions exchange, LnW$_{10}$ is extracted and transferred into organic phase. The chloroform solution is separated by funnel, and the excess chloroform was evaporated to obtain SLnW$_{10}$. The energy dispersive spectrometer (EDS) analysis of the SEuW$_{10}$ is performed to check the full replacement of Na^+ by HTAB and the result listed in the Figure S2 and Table S1. The key to understand the polymerization process of lanthanide inorganic/organic hybrid materials is the aggregation reaction between different units. While VPD is added into the compounds of HTAB modified LnW$_{10}$ and ZIF-8 to blend, VPD can coordinate to lanthanide ions through its nitrogen atoms. And after the addition of EMA, under the action of unsaturated bonds, it can aggregate with VPD to construct polymer hybrids. Finally, the final multicomponent hybrid systems are assembled through the copolymerization reaction between SLnW$_{10}$, ZIF-8 and polymer.

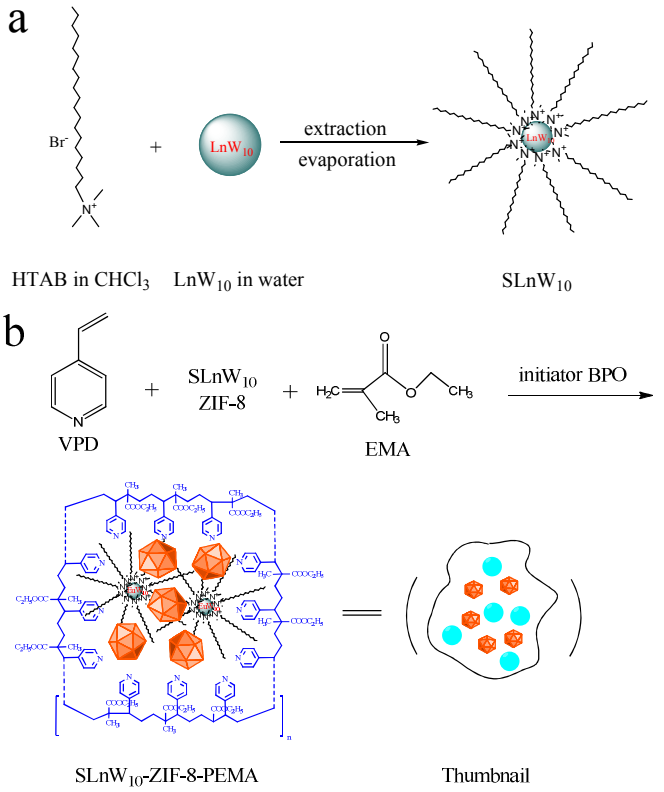

Figure 1 Selected scheme of the synthesis process of SLnW$_{10}$ (a) and SLnW$_{10}$-ZIF-8-PEMA (b), for LnSiW$_{11}$ system, it is similar.

The FT-IR spectra of HTAB, EuW$_{10}$, SEuW$_{10}$ and SEuW$_{10}$-ZIF-8-PEMA are shown in Figure 2. In the spectrum of SEuW$_{10}$, the bands at 2917, 2848 cm^{-1} belong to the asymmetric and symmetric stretching vibrations of CH_2 in HTAB long alkyl chains, respectively. And C–H bending vibration is located at 1486 cm^{-1}. SEuW$_{10}$ has almost the same band of HTAB and the partial bands of EuW$_{10}$, which suggests that HTAB surfactant has completely replaced sodium ions of EuW$_{10}$. The broad band situated at 3450 cm^{-}

RSC Advances Accepted Manuscript

[1] is related to the stretching mode of O-H, indicating the presence of water molecules and it is common phenomenon that some water molecules surround the $SEuW_{10}$ in their long alkyl chains. In addition, the stretching vibration absorption bands *v* (C=O, 1620 cm^{-1}) and *v* (C-O, 1276 and 1147 cm^{-1}) are representative of -COO- group of EMA. And the band that centered at1470 cm^{-1} of $SEuW_{10}$-ZIF-8-PEMA has relation to the asymmetric stretching vibration of C-N, which reveals the presence of 4-vinyl pyridine. Compared with $SEuW_{10}$-ZIF-8-PEMA, the band to HTAB and EuW_{10} in the spectrum of $SEuW_{10}$ can also be observed as a result of polymerization reaction. Contrasted with LnW_{10} material, they have the nearly same FT-IR spectra in the $LnSiW_{11}$ (Figure S3).

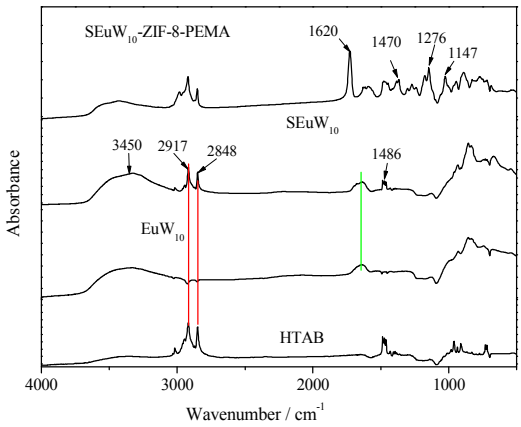

Figure 2 Selected FTIR spectra of HTAB, EuW_{10}, $SEuW_{10}$ and $SEuW_{10}$-ZIF-8-PEMA

The thermal stability of the products is examined by thermal gravimetric analysis (TGA), which is performed under air with a heating rate of 5 K/min (Figure S4). TGA data reveals that hybrid materials releases its organic components (EMA, VPD and BPO) in the temperature range of 45 ºC to 220 °C. Compound $SEuW_{10}$-ZIF-8-PEMA is thermally stable to 350 °C, above which a further mass loss of 70 wt % before 500 °C is ascribed to decomposition of the framework forming $Zn(MeIM)_2$. It is noted that no mass loss is observed between 220 and 500 °C, revealing ZIF-8 does not contain other small molecules inside the channels. Obviously, TGA indicates that the thermal stability of hybrid materials is much better in comparison with the lanthanide complexes.

The room temperature PXRD patterns from 5 to 60 ° of HTAB, EuW_{10}, $SEuW_{10}$, ZIF-8 and $SEuW_{10}$-ZIF-8-PEMA are shown in Figure 3. From the figure, we can see that the PXRD pattern of surfactant capped EuW_{10} ($SEuW_{10}$) showed almost different peaks between the bottomed original materials of HTAB and EuW_{10}, which suggests that the structure and morphology are completely changed after ions exchanging between surfactant and POMs (The PXRD patterns of HTAB, $EuSiW_{11}$, $SEuSiW_{11}$, ZIF-8 and $SEuSiW_{11}$-ZIF-8-PEMA are displayed in Figure S5). The HTAB can replace the Na^+ and surrounded them to form a hydrophobic material. In the top pattern, the diffraction peaks of $SEuW_{10}$-ZIF-8-PEMA partly agree well with the each value of EuW_{10} and ZIF-8 as-synthesized, which indicates that the products had two main components of ZIF-8 and EuW_{10}. But a little difference accompanies in the product, which may be influenced by the excess surfactant HTAB sticking on the external of EuW_{10}. At the same time, the intensity of the peaks of ZIF-8 are much stronger than the other component in the $SEuW_{10}$-ZIF-8-PEMA, which means that the doping amount of lanthanide ions is less than the ZIF-8 in the product, and ZIF-8 is the major components of the compounds. And we can predict that the intensity of lanthanide diffraction peaks may increase with the increase of $SEuW_{10}$ content.

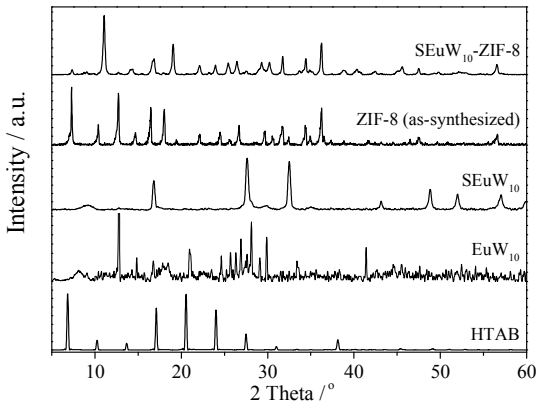

Figure 3 Wide-angle x-ray diffraction patterns of HTAB, EuW_{10}, $SEuW_{10}$, ZIF-8 and $SEuW_{10}$-ZIF-8-PEMA

The luminescence performances of lanthanide hybrid materials have been studied at room temperature. Figures S6 (a) depicts the luminescent excitation and emission spectra of the parent lanthanide polyoxometalates EuW_{10}. The excitation spectrum of EuW_{10} is monitored by 614 nm of the $^5D_0 \rightarrow {}^7F_2$ Eu^{3+} characteristic transition. The broad band locating at 300 nm is attributed to the O-W charge transfer (CT) states.[21] The excitation of ligand to metal charge transfer (LMCT) accompanies with energy transfer from ligand $[W_5O_{18}]^{6-}$ to Eu^{3+} which leads to series of Eu^{3+} characteristic emission. The various lines are caused by the interior 4f-4f transitions in the excitation spectra and the characteristic peaks of Eu^{3+} situate at 362 ($^7F_0 \rightarrow {}^5D_4$), 374 ($^7F_0 \rightarrow {}^5G_4$), 381 ($^7F_0 \rightarrow {}^5G_3$), 384 ($^7F_0 \rightarrow {}^5G_2$) and 394 ($^7F_0 \rightarrow {}^5L_6$), respectively. The $^7F_0 \rightarrow {}^5L_6$ transition at 394 nm is the strongest intensity of excitation bands, which indicates that 4f-4f transitions have higher intensity than the LMCT states. The excitation spectra of other LnW_{10} (TbW_{10}, SmW_{10} and DyW_{10}) are shown in Figures S6 (b), (c) and (d), and they are all similar to EuW_{10}, a broad band with peak at nearby 300 nm and lanthanide inner electron transitions behind. Figures S5 also shows the information of emission spectra of four parent lanthanide polyoxometalates LnW_{10}, (Ln = Eu, Tb, Sm and Dy), and the emission spectra of the other lanthanide polyoxometalates $LnSiW_{11}$, (Ln = Eu, Sm and Dy) are displayed in Figure S7. In the emission spectra of EuW_{10} and $EuSiW_{11}$ (Figure S6 (a), S6 (a)), there are four main sharp emission bands between 550 and 750 nm which reveal the characteristic transitions of Eu^{3+} ions and they are ascribed to $^5D_0 \rightarrow {}^7F_J$ (J = 1-4) transitions at about 594, 614, 652, 703 nm respectively. In emission spectrum of TbW_{10} (Figure S6 (b)), four sharp peaks in the range of 450 to 700 nm are attributed to f-f transitions of Tb^{3+} and are due to $^5D_4 \rightarrow {}^7F_6$ (488 nm), $^5D_4 \rightarrow {}^7F_5$ (545 nm), $^5D_4 \rightarrow {}^7F_4$ (583 nm) and $^5D_4 \rightarrow {}^7F_3$ (621 nm), respectively. Among these emission peaks, the prominent green luminescence

RSC Advances Accepted Manuscript

This journal is © The Royal Society of Chemistry 2012

$^5D_4 \rightarrow {}^7F_5$ was observed in their emission spectra. The characteristic narrow emission bands of SmW_{10} and $SmSiW_{11}$ which located from 550 to 750 nm are clearly showed in Figure S6 (c) and S7 (b). The peaks that split into some parallel shoulder peaks are centered about 567 (561), 607 (597), 652 (646) and 703 nm, respectively. They belong to $^4G_{5/2} \rightarrow {}^6H_J$ (J = 5/2, 7/2, 9/2, 11/2) of Sm^{3+}. Among these peaks, the orange luminescence $^4G_{5/2} \rightarrow {}^6H_{7/2}$ is the strongest. Figure S6 (d) and S7(c) show the emission spectrum of DyW_{10} and $DySiW_{11}$. The typical transitions of dysprosium ion are obviously splitting at 479 (490) and 574 (585) nm, which corresponds to $^7F_{9/2} \rightarrow {}^6H_{15/2}$ (479 nm, blue luminescence) and $^7F_{9/2} \rightarrow {}^6H_{13/2}$ (574 nm, yellow luminescence). The blue emission is more efficient than the yellow emission by comparing their relative intensities. Photoluminescence comparisons of two kinds of polyoxometalates encapsulated hybrids in ZIF-8 are discussed below.

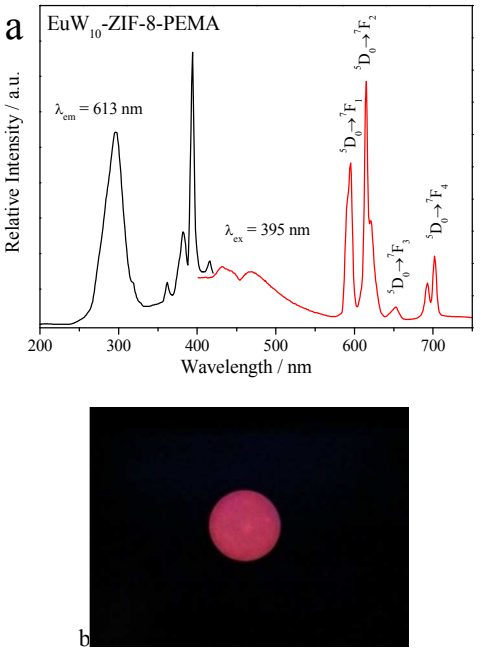

Figure 4 The excitation and emission spectra of $SEuW_{10}$-ZIF-8-PEMA (a) and the digital photograph of $SEuW_{10}$-ZIF-8-PEMA by a 395 nm irradiated in dark (b).

Figure 4 (a) shows the luminescence spectra of hybrids with $SEuW_{10}$-ZIF-8-PEMA. The excitation spectra of the hybrids are monitored by selecting the characteristic emission band of the Eu^{3+} ion at 613 nm, also with large broad band ranging from 250-350 nm. Besides, it is obvious that strong and sharp lines existed in 330–500 nm range are attributed to the interior narrow 4f-4f transitions of Eu^{3+} in the host lattice. In the excitation spectra, the front broad band is ascribed to the O-W charge transfer of the tungstate above-mentioned. The center of broad band in $SEuW_{10}$-ZIF-8-PEMA blue-shift to about 290 nm from the central 300 nm of the parent EuW_{10} (the hybrid of $SEuSiW_{11}$-ZIF-8-PEMA have the same and further blue-shift phenomenon from 350 to 330 nm in Figure S8 (a)). And the excitation spectrum of the two hybrids showing characteristic peaks of Eu^{3+} is much stronger than the LMCT band. Comparing the two main kinds of excitation spectra of ZIF-8 and EuW_{10}, they have the same excitation bands at 390 nm approximately (the luminescent excitation and emission spectra of ZIF-8 is shown in Figure S9). While monitored the emission wavelength under 395 nm, both of the two materials are appealed in the emission luminescent spectra of $SEuW_{10}$-ZIF-8-PEMA. The digital photograph of the sample is checked by exciting at 395 nm (Figure 4 (b)). The weak blue emissions between 430 and 500 nm are assigned to the ZIF-8, and a dominant red emission is observed between 580 and 710 nm originating from the EuW_{10} above-mentioned, respectively. The integration luminescence appears pink in color, which is due to a combination of blue and red emissions from the two materials. The $SEuSiW_{11}$-ZIF-8-PEMA displays a blue-white color and digital photograph shows in Figure S8 (b).

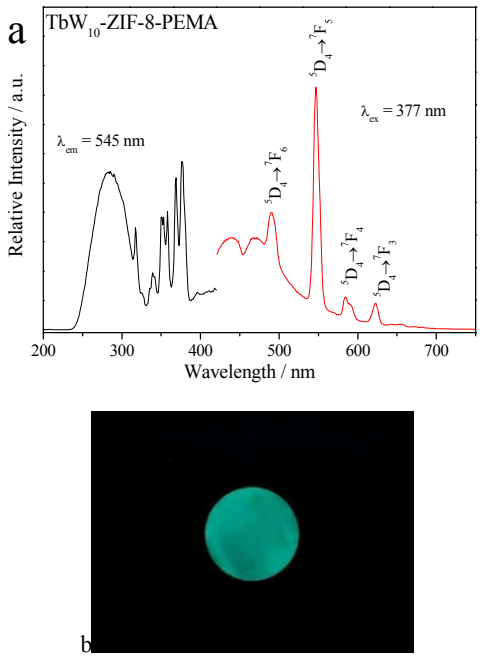

Figure 5 The excitation and emission spectra of $STbW_{10}$-ZIF-8-PEMA (a) and the digital photograph of $STbW_{10}$-ZIF-8-PEMA by a 377 nm irradiated in dark (b).

Figure 5 (a) shows the photoluminescence spectra of terbium hybrid $STbW_{10}$-ZIF-8-PEMA. The excitation spectrum is collected by characteristic emission wavelength of 545 nm of Tb^{3+} ion, and a broad band between 320 and 400 nm with the maximum peak of approximately 377 nm originates from Tb^{3+} 4f–4f direct excitation. The emission spectrum of it is also excited by the maximum excitation wavelength of characteristic peaks of Tb^{3+}. Although the broad band O-W ligands-metal charge transfer transition has a strong intensity, it is not allowed to excite the emission of ZIF-8 at the same time. In the emission spectrum of the hybrids, the blue luminescence at 485-495 nm is due to $^5D_4 \rightarrow {}^7F_6$ transition and the strongest peaks 545 nm is ascribed to $^5D_4 \rightarrow {}^7F_5$ transition. Other two weak peaks in the orange luminescence region at 585 nm and the red at 623 nm are related to $^5D_4 \rightarrow {}^7F_4$ and $^5D_4 \rightarrow {}^7F_3$ transition, respectively. Besides the characteristic emission of Tb^{3+}, a broad band locating at the range of 420 ~ 470 nm in the blue region is assigned to the emission of ZIF-8. Figure 5 (b) shows the digital

RSC Advances Accepted Manuscript

photograph of the sample under the excitation conditions. The final luminescence displays light blue color for a combination of green and blue emissions from the TbW_{10} and ZIF-8 respectively.

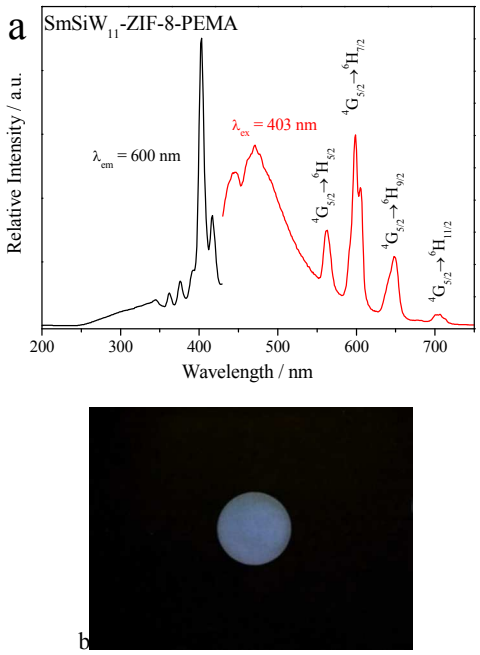

Figure 6 The excitation and emission spectra of $SSmSiW_{11}$-ZIF-8-PEMA (a) and the digital photograph of $SSmSiW_{11}$-ZIF-8-PEMA by a 403 nm irradiated in dark (b).

We study the photoluminescence property of hybrids of $SSmW_{10}$-ZIF-8-PEMA and $SSmSiW_{11}$-ZIF-8-PEMA. Figure S10 (a) shows the excitation spectra monitored at 600 nm and the emission spectra obtained by the excitation of LMCT at room temperature. The emission spectra show three bands of emission transitions as the result of the introduction of tungstate. Tungstate leads to the split of $^4G_{5/2}\rightarrow{}^6H_{5/2}$, $^4G_{5/2}\rightarrow{}^6H_{7/2}$, $^4G_{5/2}\rightarrow{}^6H_{9/2}$ transitions. The transition $^4G_{5/2}\rightarrow{}^6H_{5/2}$ at 568 nm divide from 561 to 568 nm, another transition $^4G_{5/2}\rightarrow{}^6H_{7/2}$ at 608 nm split from 600 nm to 608 nm and the last observed transition $^4G_{5/2}\rightarrow{}^6H_{9/2}$ at 653 nm break into emission region from 646 nm to 653 nm. Among three emission bands, the transition $^4G_{5/2}\rightarrow{}^6H_{7/2}$ is of the highest intensity. The emission spectra of $SSmW_{10}$-ZIF-8-PEMA only shows the red color of the matrix by the excitation of LMCT and the photograph shows in the Figure S10 (b). When monitored the emission wavelength under 395 nm of the characteristic peak of ZIF-8, only another matrix is appealed in the emission luminescent spectra of $SSmW_{10}$-ZIF-8-PEMA and blue photograph in the Figure S10 (c). $SSmW_{10}$-ZIF-8-PEMA becomes a material which can appeal different luminescence under different excitation. But in the hybrid of $SSmSiW_{11}$-ZIF-8-PEMA, due to the different POM, it has different photoluminescence feature. The excitation spectrum of $SSmSiW_{11}$-ZIF-8-PEMA is collected by 600 nm which is a Sm^{3+} ions characteristic emission wavelength, and a narrow band between 390 and 420 nm with the maximum peak of approximately 403 nm that is attributed to the interior narrow 4f-4f transitions of Sm^{3+}. So in the emission spectrum of $SSmSiW_{11}$-ZIF-8-PEMA, both of the two materials can be observed and the digital photograph of the hybrids shown in Figure 6 (b) under excited at 403 nm. A dominant red emission locating between 580 and 710 nm is originated from the $SmSiW_{11}$ afore-mentioned; a blue emission between 430 and 490 nm is ascribed to the ZIF-8. The integration luminescence displays white color, owing to a combination of blue and red emissions from the two materials, respectively.

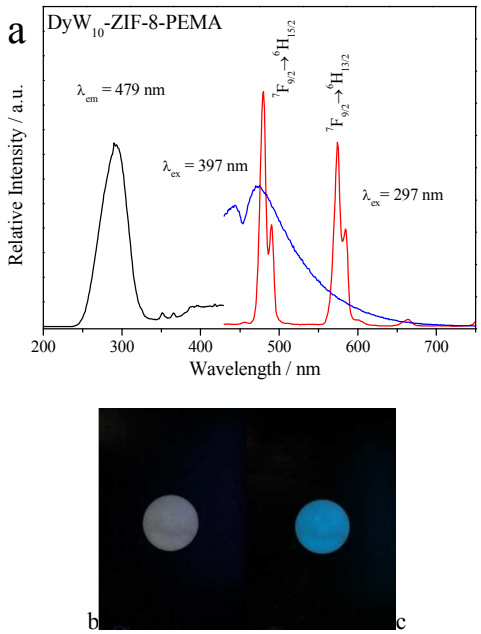

Figure 7 The excitation and emission spectra of $SDyW_{10}$-ZIF-8-PEMA (a), the digital photograph of $SDyW_{10}$-ZIF-8-PEMA by a 297 nm irradiated (b) and 397 nm (c) in dark, respectively.

The luminescence features of $SDyW_{10}$-ZIF-8-PEMA and $SDySiW_{11}$-ZIF-8-PEMA incorporating DyW_{10} and $DySiW_{11}$ are presented in Figure 7 (a) and Figure S11 (a), respectively. Two excitation spectra are both obtained by monitoring the $^7F_{9/2}\rightarrow{}^6H_{15/2}$ transition at 479 nm. In the excitation spectra of $SDyW_{10}$-ZIF-8-PEMA, the broad band of O-W ligands-metal charge transfer transition contributes more than lanthanide characteristic excitation lines, showing high intensity of the LMCT as well as $SSmW_{10}$-ZIF-8-PEMA. Whereas in the excitation spectra of $SDySiW_{11}$-ZIF-8-PEMA, the relative intensity of characteristic excitation lines of the Dy^{3+} 5f–5f transitions is more intense than the O-W ligands-metal charge transfer transition. The emission spectrum of $SDyW_{10}$-ZIF-8-PEMA has the similar feature to that $SSmW_{10}$-ZIF-8-PEMA and only shows white luminescence by the excitation of LMCT (photograph shown in Figure 7 (b)). The emission assembles the characteristic emission of DyW_{10} in positions, shapes, width, with split peaks of $^7F_{9/2}\rightarrow{}^6H_{15/2}$, $^7F_{9/2}\rightarrow{}^6H_{13/2}$ transitions in the range of 479-490 nm, 574-585 nm, correspondingly. Meanwhile the blue luminescence is stronger than the yellow one. ZIF-8 as the other component the emission wavelength is monitored by 397 nm of its characteristic peak, and blue photograph in the Figure 7 (c). In the hybrid of $SDySiW_{11}$-ZIF-8-PEMA, its luminescence phenomenon has different from $SDyW_{10}$-ZIF-8-PEMA because incorporating different matrix. The excitation spectrum of $SDySiW_{11}$-ZIF-8-PEMA was monitored by 479 nm that is one of the characteristic

RSC Advances Accepted Manuscript

This journal is © The Royal Society of Chemistry 2012

emission wavelengths of Dy^{3+} ions, and accompanying series bands 340 to 420 nm with the maximum value of nearly 366 nm which is ascribed to the interior 5f-5f transitions of Dy^{3+}. And two main components can be observed in the emission spectrum of $SDySiW_{11}$-ZIF-8-PEMA in Figure S11 (a) and the digital photograph of the hybrid showed in Figure S11 (b) under 366 nm to excite. There are two dominant blue and yellow luminescence located at the range of 479-490 nm and 574-585 nm respectively which derivate from the $DySiW_{11}$ mentioned. And a tiny blue emission between 420 and 470 nm was attributed to the ZIF-8. The integration luminescence displays blue-white color which is combined of a light-blue (trace amounts of ZIF-8 in the hybrids) and white emissions from the two components, respectively.

Table 1 Luminescence lifetimes and absolute quantum yields of $SLnW_{10}$-ZIF-8-PEMA and $SLnSiW_{11}$-ZIF-8-PEMA

LnW_{10}/$LnSiW_{10}$	τ (μs)	η(%)	λex(nm)	λem(nm)
EuW_{10}	1017	24.3	395	613
TbW_{10}	936	17.7	377	545
SmW_{10}	54	10.6	295	600
DyW_{10}	55	9.1	297	479
$EuSiW_{11}$	938	19.9	394	613
$SmSiW_{11}$	100	11.4	403	600
$DySiW_{11}$	74	9.2	366	479

The transmission electron microscopy (TEM) analysis has been provided in Figure S12. In the TEM, we can see that the process of ions exchanging make LnW_{10}/$LnSiW_{11}$ into nanoparticles and the inorganic components of $SLnW_{10}$/$SLnSiW_{11}$ and ZIF-8 are homogeneous diffused into the organic matrices. The photographs of the thin films are given in Figure S13. The photographs display the transparency of the films of $SEuW_{10}$-ZIF-8-PEMA and $SEuSiW_{11}$-ZIF-8-PEMA respectively. The excitation wavelength, luminescence lifetimes and emission quantum yields are listed in Table 1. From the data, it can be seen that the hybrid films fabricated with EuW_{10} and $EuSiW_{11}$ possess the longer lifetimes and higher quantum yields than other hybrid systems.

Conclusions

We have prepared two kinds of lanthanide polyoxometalates ($Na_9LnW_{10}O_{36}\cdot 32H_2O$, $K_{13}Ln(SiW_{11}O_{39})_2\cdot 30H_2O$ (Ln = Eu, Tb, Sm, Dy) and encapsulated polyoxometalate into surfactant to obtain surfactant-encapsulated POM clusters ($SLnW_{10}$/$SLnSiW_{11}$) and zeolitic imidazolate frameworks ZIF-8. In the presence of benzoyl peroxide (BPO) as the initiator, the synthesized surfactant-encapsulated POMs, ZIF-8 and polymer units are composed by additional polymerization reaction. The photoluminescent properties of these hybrids show that hybrids containing EuW_{10} or $EuSiW_{11}$ both have longer lifetimes and higher quantum yields than other lanthanide hybrids. And some of the hybrid systems appeal almost cool-white emission. $SSmW_{10}$-ZIF-8-PEMA and $SDyW_{10}$-ZIF-8-PEMA can carry out emitting different luminescence under different excitation. $SEuW_{10}$-ZIF-8-PEMA, $SEuSiW_{11}$-ZIF-8-PEMA and $SSmSiW_{11}$-ZIF-8-PEMA hybrids in particular can be expected to have potential value in practical cool-white lighting. This provides a new strategy to obtain white luminescence hybrid materials.

Acknowledgements

This work was supported by the National Natural Science Foundation of China (91122003) and Developing Science Funds of Tongji University.

Notes and references

Department of Chemistry, Tongji University, Siping Road 1239, Shanghai 200092, China.Fax: +86-21-65981097; Tel: +86-21-65984663; E-mail: byan@tongji.edu.cn

Electronic Supplementary Information (ESI) available: [details of any supplementary information available should be included here]. See DOI: 10.1039/b000000x/

‡ Footnotes should appear here. These might include comments relevant to but not central to the matter under discussion, limited experimental and spectral data, and crystallographic data.

1 (*a*) W. H. Green, K. P. Le, J. Grey, T. T. Au and M. J. Sailor, *Science*, 1997, **276**, 1826; (*b*) P. C. R. Soares-Santos, H. I. S. Nogueira, V. Felix, M. G. B. Drew, R. A. S. Ferreira, L. D. Carlos and T. Trindade, *Chem. Mater.*, 2003, **15**, 100; (*c*) L. D. Carlos, R. A. S. Ferreira, V. D. Bermudez and S. J. L. Ribeiro, *Adv. Funct. Mater.*, 2001, **11**, 111; (*d*) C. Sanchez, G. J. D. A. Soler-Illia, F. Ribot, T. Lalot, C. R. Mayer and V. Cabuil, *Chem. Mater.*, 2001, **13**, 3061.

2 (*a*) P. Escribano, B. Julian-Lopez, J. Planelles-Arago, E. Cordoncillo, B. Viana and C. Sanchez, *J. Mater. Chem.*, 2008, **18**, 23; (*b*) L. D. Carlos, R. A. S. Ferreira, R. N. Pereira, M. Assuncao and V. D. Bermudez, *J. Phys. Chem. B*, 2004, **108**, 14924; (*c*) L. S. Fu, R. A. S. Ferreira, S. S. Nobre, L. D. Carlos and J. Rocha, *J. Lumin.*, 2007, **122**, 265.

3 (*a*) J. Cuan and B. Yan, *Dalton Trans.*, 2013, **42**, 14230; (*b*) B. Yan, *RSC Adv.*, 2014, **4**, 1735.

4 (*a*) C.L. Hill,*Chem. Rev.*,1998, **98**,1; (*b*) M. T. Pope and A. Müller, *Angew. Chem. Int. Ed.*, 1991, **30**, 34.

5 (*a*) T. Yamase, E. Ishikawa, K. Fukaya, H. Nojiri, T. Taniguchi and T. Atake, *Inorg Chem.*, 2004, **43**, 8150; (*b*) N.Casañ-Pastor and P.Gómez-Romero,*FrontiersinBioscience*, 2004,**9**, 1759; (*c*)V. Luca and J. M. Hook, *Chem. Mater.*, 1997, **9**, 2731.

6 (*a*) E. Coronado and C. Mingotaud, *Adv. Mater.*, 1999, **11**, 869; (*b*) M. Chemente-leon, B. Agricole, C. Mingotaud, C. J. Gomez-Garcfa, E. Coronado and P. Delhaes, *Angew. chem., Int. Ed. Engl.*, 1997, **36**, 1114.

7 R. D.Peacock and T. J. R.Weakley, *J. Chem. Soc. A*, 1971, 1836.

8 (*a*) M. Sugeta and T. Yamase, *Bull. Chem. Soc. Jpn.*, 1993, **66**, 444; (*b*) K. Binnemans, *Chem. Rev.*, 2009, **109**, 4283.

9 G. Decher, *Science*, 1997, **277**, 1232.

10 (*a*) W. F. Bu, L. X. Wu and A. Q. Tang, *J. Coll. Interf. Sci.*, 2004, **269**, 472; (*b*) Y. Y. Zhao, Y. Li, W. Li, Y. Q. Wu and L. X. Wu, *Langmiur*, 2010, **26**, 18430.

11 (*a*) W. Bu, J. Zhang, L. Wu and A. C. Tang, *Chin. J. Chem.*, 2002, **20**, 1514; (*b*) W. Bu, L. Wu, X. Hou, H. Fan, C. Hu and X. Zhang, *J. Colloid Interface Sci.*, 2002, **251**, 120.

12 (*a*) S. Polarz, B. Smarsly and M. Antonietti, *Chem. Phys. Chem.*, 2001, **1**, 457; (*b*) D. Volkmer, A. Du Chesne, D. G. Kurth, H. Schnablegger, P. Lehmann, M. J. Koop and A. Müller, *J. Am. Chem. Soc.*, 2000, **122**, 1995; (*c*) D. G. Kurth, P. Lehmann, D. Volkmer, H. Cölfen, M. J. Koop, A. Müller and A. Du Chesne, *Chem. Eur. J.*, 2000, **6**, 385.

13 (*a*) O. M. Yaghi, M. O'Keeffe, N. W. Ockwig, H. K. Chae, M. Eddaoudi and J. Kim, *Nature*, 2003, **423**, 705; (*b*) Horike, S. Shimomura and S. Kitagawa, *Nat. Chem.*, 2009, **1**, 695.

14 K. S. Park, Z. Ni, A. P. Cote, J. Y. Choi, R. D. Huang, F. J. Uribe-Romo, H. K. Chae, M. O'Keeffe and O. M. Yaghi, *PNAS*, 2006, **103**, 10186.

15 B. Wang, A. P. Cote, H. Furukawa, M. O'Keeffe and O. M. Yaghi, *Nature*, 2008, **453**, 207-211.

16 (*a*)W. Qi and L. Wu, *Polymer International*, 2009, **58**, 1217; (*b*)M. Amela-Cortes, A. Garreau, S. Cordier, E. Faulques, J.-L. Duvail and Y. Molard, *J. Mater. Chem. C*, 2014, **2**, 1545; (*c*)Y. Molard, F. Dorson, K. A. Brylev, M. A. Shestopalov, Y. Le Gal, S. Cordier, Y. V. Mironov, N. Kitamura and C. Perrin, *Chem.-Eur. J.*, 2010, **16**, 5613.

RSC Advances Accepted Manuscript

17 (*a*) T. R. Zhang, C. Spitz, M. Antonietti and C. F. J. Faul, *Chem. Eur. J.*, 2005, **11**, 1001; (*b*) G. Hungerford, M. Green and K. Suhling, *Phys. Chem. Chem. Phys.*, 2007, **9**, 6012.
18 J. N. Hao and B. Yan, *Dalton Trans.*, 2014, **43**, 2810.
19 Y. Zhou and B. Yan, *Inorg. Chem.*, 2014, **53**, 3456.
20 (*a*) R. A. S. Ferreira, S. S. Nobre, C. M. Granadeiro, H. I. S.Nogueira, L. D. Carlos and O. L. Malta, *J. Lumin.*, 2006, **121**, 561; (*b*) H. Naruke and T. Yamase, *J. Lumin.*, 1991, **50**, 55.
21 J. Wang, H. S. W., L. S. Fu, F. Y. Liu and H. J. Zhang, *Thin Solid Films*, 2002, **414**, 256.

RSC Advances Accepted Manuscript

 This journal is © The Royal Society of Chemistry 2012